


PSFC/JA-01-27

**Evolution of Pedestal Profiles through the
L-H and H-L Transitions in Alcator C-Mod**

View metadata, citation and similar papers at core.ac.uk

brought to you by  **DSpace**
provided by DSpace

E.S. Marmor, D. Mossessian, S. Wukitch

October 2001

Plasma Science and Fusion Center
Massachusetts Institute of Technology
Cambridge, MA 02139 USA

¹Oak Ridge National Laboratory, Oak Ridge, TN, 37831

This work was supported by the U.S. Department of Energy, Cooperative Grant No. DE-FC02-99ER54512. Reproduction, translation, publication, use and disposal, in whole or in part, by or for the United States government is permitted.

Submitted for publication to *Plasma Physics and Controlled Fusion*.

**Evolution of Pedestal Profiles through the L-H and H-L Transitions
in Alcator C-Mod**

A. E. Hubbard, B. A. Carreras*, R.L. Boivin, J. W. Hughes, E. S. Marmor,
D. Mossessian, S. Wukitch

MIT Plasma Science and Fusion Center, Cambridge, MA 02139, USA
*Oak Ridge National Laboratory, Oak Ridge, TN 37831, USA

ABSTRACT

Local edge electron parameters are measured in the Alcator C-Mod tokamak, during discharges in which input power is continuously ramped up and down, leading to transitions from the low-confinement (L) to high confinement (H) mode and back to L-mode. This allows measurement of the accessible portions of the non-monotonic flux-gradient relationship proposed by models of the H-mode as a critical transition. Results are consistent with a dependence of conductivity χ on temperature gradient, having a very sharp decrease above a critical value. Other possible flux-gradient relations are also examined, and the data are compared with theoretical formulations. The initial transient of pedestal energy in the first few ms after the L-H transition is also analysed and found to be consistent with a sudden decrease in χ across the pedestal region.

Submitted to *Plasma Physics and Controlled Fusion*
September 2001

Corresponding Author:

Amanda Hubbard

MIT Plasma Science and Fusion Center, NW17-113

175 Albany St., Cambridge MA 01239, USA

Hubbard@psfc.mit.edu

Tel: (617)253-3220

Fax: (617)253-0627

1. Introduction

In studying the transition mechanism from a low confinement mode (L-mode) to a high confinement (H-mode), three levels of time scales can be considered. There is the fast time scale of the transition (of the order of 100 μ s). A great deal of effort has been dedicated to get diagnostics on this time scale, to determine the cause of the transition by observing a succession of fast changes in the parameters¹. However, if the L to H transition is a critical transition such a chain of causal events does not necessarily exist. Less attention has been paid to the other time scales in the transition process. There is an intermediate time scale, of the order of milliseconds, in which the density and temperature profiles respond to the transition. Finally, one can consider the evolution of different equilibria responding to changes in the power and going through the full hysteresis cycle L–H–L. Exploration of these scales provides important information on the nonlinear structure of the fluxes, which is essential to understand in order to explain the bifurcation properties.² In this paper, we will consider these last two time scales and try to address some questions about the transition that can be provided by the plasma response. The Alcator C-Mod tokamak³ is well suited to such studies, since it has a flexible ICRF power heating system that allows us to slowly and continuously vary the power across the transition threshold and then follow a controlled evolution back to L-mode. There is also an extensive set of pedestal diagnostics, described in the following section. This paper focusses on measurements of local fluxes and gradients on the slow, quasi-equilibrium, time scale. Possible functional relations are examined and compared to theoretical formulations in Section 3. The faster transient in the first few ms after the L-H transition is briefly discussed in Section 4.

2. Description of the experiments.

Dedicated threshold experiments were carried out on the Alcator C-Mod tokamak, at a toroidal field of 5.4 T and plasma current of 0.8 MA. Under these conditions, with $q_{95} \sim 4.7$, H-modes are typically in the 'Enhanced D-alpha' (EDA) regime, in which continuous, quasi-coherent edge fluctuations enhance the particle transport over ELM-free levels, leading to steady density and impurity levels⁴. ICRF power at 80 MHz is ramped up and down linearly, as shown in Figure 1, leading to an L-H and subsequent H-L transition. A range of ramp rates and power levels, up to 2.6 MW, have been used, in two separate run campaigns. The line averaged L-mode target density \bar{n}_e was also varied, from 1.2-2.2 $\times 10^{20} \text{ m}^{-3}$. The net power flux Q at the top of the edge pedestal is derived assuming 70-80% RF absorption, adding the ohmic power, and subtracting the radiation within the pedestal region, measured by bolometer arrays.

The pedestal diagnostics available on Alcator C-Mod are described in detail elsewhere⁵. Because of the high-density characteristic of the Alcator C-mod plasmas, we assume that $T_e = T_i$ and work with electron channel measurements. For fast time resolution, $\delta t \sim 1 \text{ ms}$, we use T_e from electron cyclotron emission (ECE) and density derived from visible bremsstrahlung emissivity (VB), assuming constant Z_{eff} . Since the 9-channel ECE instrument is insufficient to resolve the pedestal, core gradients were extrapolated to a radius of $\psi = 0.95$, which is typically near the top of the pedestal, to estimate $T_{\text{ped}}(t)$ and derive the averaged gradients ∇T_{eff} between this point and the separatrix. $n_{\text{ped}}(t)$ is taken at

the same location. Typical time evolution of these parameters is shown in Fig. 1. In the most recent campaign, these diagnostics were supplemented by an edge Thomson scattering (ETS) diagnostic with 1.5 mm resolution, providing pedestal profiles of n_e and T_e every 33 ms⁶. ETS profiles were used to cross-check the extrapolated values at $\psi = 0.95$, as well as to measure the maximum pedestal gradients. These are typically a factor of two higher than the averaged gradients, but have a similar time dependence. Due to the statistical uncertainties inherent in Thomson scattering, however, they tend to have larger variation between time points.

3. Flux - gradient relationship over long time scales

The evolution of the plasma edge density and temperature on a slow time scale during power ramps can be considered as a sequence of equilibria at different heat fluxes. We can then explore the structure of the flux as a function of the gradients in n and T . Most models proposed for the L-H mode transition, recently reviewed by Connor and Wilson⁷, give a non-linear, double-valued function of flux versus edge gradients, through a bifurcation in transport above some critical gradient. These models differ in the fluxes (either power or particle) which are proposed to control the transition, in the gradients which control the transport, and in the functional form of the decrease in transport coefficients. The choice of variables for this analysis is guided by experiment as well as theory. Since the H-modes were triggered by ramping up P_{RF} at constant n_e , power appears more important than particle flux in this case. Noting that $T_{e,ped}$ in Fig. 1 responds to power in both L and H-mode, while the density shows a bifurcation at the transitions but is otherwise nearly independent of power, it seems that the local parameter controlling the transport must include temperature (eg. ∇T or ∇p). This is consistent with previous studies on C-Mod which have shown that for fixed plasma configuration, there is a threshold value of edge temperature at the L-H transition⁸. Since T_e at the separatrix is nearly constant due to SOL power balance, $T_{e,95}$ and ∇T are closely linked^{8,9}.

The prevalent theoretical picture of transport barrier formation is that it is due to $E \times B$ shear flow suppression of turbulence. In this case the relevant variable is du_E/dr , where $u_E \equiv cE_r/B$ is the $E \times B$ flow and E_r is the radial electric field. An expression of the thermal conductivity that includes the effect of shear flow suppression of the form

$$\mathbf{c} = \mathbf{c}_H + \frac{\mathbf{c}_a}{1 + \mathbf{a} (du_E / dr)^g} \quad (3.1)$$

has been proposed^{10,11}, where χ_a is the anomalous thermal conductivity, χ_H is the reduced level in the H-mode barrier, and α and γ are constants. However, u_E is not measured directly on C-Mod or most other experiments, so various approximations have been made. In Ref. 10, Hinton assumes that χ is the sum of the ion neoclassical contribution and a turbulent contribution modified by the poloidal rotation shear, which can be expressed in terms of ∇T resulting in

$$\mathbf{c} = \mathbf{c}_H + \frac{\mathbf{c}_a}{1 + \mathbf{I}_a (\nabla T / \nabla r)^4} \quad (3.2)$$

In Ref. 11, in contrast, Hinton and Staebler neglect the poloidal and toroidal flow terms

and also the second order derivatives, giving

$$\frac{du_E}{dr} \simeq -\frac{c}{eBn_i^2} \frac{dn_i}{dr} \frac{dp_i}{dr} \quad (3.3)$$

They assume that $\gamma = 2$, that n_i is weakly varying in time and the temperature gradient dominates over the density gradient, giving

$$\mathbf{c} = \mathbf{c}_H + \frac{\mathbf{c}_a}{1 + \mathbf{a} (dn_i/dr)^2 (dT_i/dr)^2} \quad (3.4)$$

However, in our experiment $n_{e,ped}$ varies significantly and, since $n_{e,sep}$ is roughly constant, it tends to cancel out much of the variation in dn/dr and dp/dr . One can instead write Eq.

3.3 as $\frac{du_E}{dr} = -\frac{c}{eB} \frac{1}{L_n} \left(1 + \frac{L_T}{L_n}\right) \frac{dT}{dr}$. If one neglects the variation in the density and

temperature scale lengths L_n and L_T instead of in the absolute density, a dependence of χ on dT/dr similar to Eq. 3.2 is obtained, but with an exponent $\gamma = 2$ instead of 4.

A dynamical model coupling fluctuation evolution to the flow and pressure transport has also been proposed¹². In this model, there is no simple expression for the effective nonlinear diffusivity. However, by slaving the fluctuations to the shear flow one gets a simple relation between the rms fluctuation level, which is proportional to the turbulence diffusivity D_a in this model, and the shear flow. This gives an expression for the diffusivity:

$$D = D_H + D_a \left[1 - \mathbf{a} (|dn/dr|)^3\right] \Theta \left[1 - \mathbf{a} (|dn/dr|)^3\right] |dn/dr| \quad (3.5)$$

Here, Θ is the Heaviside function that models the shear flow suppression of turbulence. This model considered only particle fluxes and density gradients for simplicity, but should also apply to the more general case of thermal transport. Recently it has been pointed out that second derivatives of n and/or T should be important for suppression of turbulence, which would add an additional term to the denominator of Eq. 3.2 or 3.4 and could alter the form of the flux-gradient relation significantly¹³. However, as second derivatives cannot be measured with sufficient accuracy, we restrict ourselves for this initial study to considering first-order gradients, and the functional forms proposed above.

Assuming that half of the power flows through the electron channel, the local power balance is given by $Q/2A = -\mathbf{c}_{eff} n_e k \nabla T_e$, where A is the plasma surface area and k is the Boltzmann constant. In Fig. 2, $-\nabla T_{eff}$ from ECE is plotted against $Q/2kAn_{e,ped}$ at 5 ms intervals. The slope of the curve thus gives χ_{eff} directly, an advantage of plotting vs the gradient rather than T_e , and the decrease from L to H-mode is clearly evident. Figure 2(a) is for an L-mode target density $\bar{n}_e = 1.1 \times 10^{20} \text{ m}^{-3}$, with points from two discharges combined to give a larger range of input power, while 2(b) is from two higher density discharges with $\bar{n}_e = 2.2 \times 10^{20} \text{ m}^{-3}$. The open diamonds indicate time points in which T_e , n_e and/or input power are changing rapidly and conditions are not in equilibrium, and are not used in fits. The curves represent best fits to the other points (+), assuming χ_{eff} depends only on ∇T . The dashed line (Fit A) uses Eq. 3.2, ie. taking $\gamma=4$, while the solid line (Fit B) represents Eq. 3.5, but with dT/dr used rather than dn/dr . The free parameters are χ_a ,

χ_H , and a 'threshold' gradient ∇T_c , which sets the constants α and λ_a . Both fits give similar values for χ_a (0.53-0.8 m²/s) and χ_H (0.09-0.12 m²/s), with no significant variation with density. Eq. 3.5 has a sharper drop in χ above the threshold, and gives a somewhat better fit to the data; $\gamma=6$ would be required in Eq 3.2 to give a similar fit, while $\gamma=2$, as assumed in Ref. 11, gives too gradual a change with ∇T . ∇T_c for each fit shows little variation between low and high-density cases, consistent with this being a fundamentally important parameter for the transition. The 'critical' values are 10.6 and 10.7 keV/m respectively for Fit A, and 18.6 and 16.4 keV/m for Fit B.

Dependences on other gradients are also possible. In Fig. 3 we plot the same dataset, but with the horizontal axis $-n_e \nabla T_e$, which approximates the average pressure gradient. The vertical axis is now $Q/2A$, so that the slope again represents χ_{eff} . This again shows a bifurcation in transport, but, since density increases in H-mode, the dependence on $n_e \nabla T_e$ does not have to be so sharp. In this case the functional form of Eq. 3.2 gives the better fit. However, the 'threshold' value of $n_e \nabla T_e$ is $\sim 40\%$ higher in the higher density data set, so that if pressure gradient is the controlling variable, one would have to postulate a threshold which increases with n_e .

Power ramp experiments were recently repeated with edge Thomson scattering, which allows more accurate evaluation of gradients. Figure 4 is for a discharge with very similar conditions to that of 2(a). If n and T from ETS at $\psi=0.95$ are used, results are very similar to those in Figs. 2 and 3. Figure 4(a) shows $Q/2kAn_e$ vs ∇T , as in Fig. 2, where the gradients and n_e are in this case evaluated at the pedestal midpoints. This choice gives systematically larger χ_{eff} values, but the functional dependence, and the threshold gradient, is consistent with that measured using ECE and VB. The higher spatial resolution of ETS also makes it possible to evaluate dependences on more complicated variables, such as du_E/dr from Eq. 3.3, without approximating the scale lengths L_N or L_T . The horizontal axis in Fig. 4(b) is $X \equiv 1/n_e^2 (dn_e/dr)_{\text{max}} (dp_e/dr)_{\text{max}}$. In order that the slope of the curves still approximately represents χ_{eff} , the vertical axis in this case is $3Q/2kAn_e L_n$ where $L_n \equiv n_e/\nabla n_{\text{max}}$ and the factor of 3 accounts roughly for $(1+L_T/L_n)$. One can also see a bifurcation of χ between L and H modes using this variable. The solid and dashed curves represent the same functional dependences considered above, while the dotted curve (Fit C) is for $\gamma=2$ as in Eq. 3.4. The higher scatter in the gradients, however, tends to obscure the dependence on flux in each regime; X can vary by a factor of two between adjacent time points and one cannot easily determine X_{crit} or choose the best fit among the various functions plotted.

4. Intermediate time response to the L-H transition.

In looking for the profile response to the transition in the intermediate time scale range, two main scenarios emerge in theoretical models of the dynamics near the L-H transition^{1,2,7,14}. In one, the transition happens in a very narrow radial region at the plasma edge and propagates inwards building up the pedestal. This propagation rate depends on how much

the power flux $\Gamma_0 = Q/A$ exceeds the critical flux Γ_c and time response of the change in energy density $p(t) = nkT$ at the pedestal is given by¹⁵ $\tilde{p}_p(t) \approx t [(\Gamma_0 - \Gamma_c)/a]$.

An alternative scenario shows the transition happening simultaneously over the broad radial range, $x_T < x < a$, of the whole pedestal. The response of the energy density in this case can be evaluated from intermediate asymptotics¹⁶. For the time scales of interest,

$$\tilde{p}(x, t) = \Gamma_0 \left(1 - \frac{c_H}{c_A} \right) \sqrt{\frac{t}{c_H}} \Phi \left(\frac{x}{\sqrt{c_H t}} \right) \quad (4.1)$$

where Φ is a dimensionless function $\Phi(y) = \frac{2}{\sqrt{p}} e^{-\frac{y^2}{4}} - y \left(1 - \frac{2}{\sqrt{p}} \int_0^y e^{-y^2} dy \right)$. The dominant time response is given by the \sqrt{t} factor multiplying Φ in Eq. (4.1).

We have attempted to explore these differences experimentally using the time response of n_e and T_e . If the plasma responds to the incremental flux, $\Gamma_0 - \Gamma_c$, one would expect that the initial rate of rise $d\tilde{p}/dt$ to depend on the rate at which the power is ramped through the threshold. Instead, it was found to be independent of dG/dt , over a wide range of the ramping rate. The magnitude of $\tilde{p}(t)$ at the top of the pedestal is consistent with Eq. 4.1, taking $x \ll \sqrt{c_H t}$ and using values of χ estimated in the previous section⁵. The transients $\tilde{p}(t)$ have also been fit with functions of the form $C t^\beta$. The derived exponent β shows considerable variation from discharge to discharge, lying typically between 0.5 and 1.0. Details of this analysis, including possible systematic dependences of β , will be reported in a separate publication. In summary, while the rates of rise in pressure are more consistent with a near-instantaneous drop in χ across the pedestal, we cannot rule out some rapid propagation of the 'front' or other, perhaps combined, scenario.

5. Discussion and Conclusions

The power ramp experiments reported here have shown that one can extract more information by following local parameters during the whole L-H-L cycle than by simply assessing parameters at the transition, as has been previously done for data from C-Mod and several other tokamaks^{8, 9, 17}. The disadvantage is that dedicated discharges are required, so that fewer transitions can be studied; the two approaches are thus complementary. For the new C-Mod data, it has been shown that plotting Q/n vs ∇T gives a consistent, strongly double-valued function. The slope χ_{eff} drops by at least a factor of six between L and H-mode, above a threshold of $\nabla T_{\text{crit}} \sim 11$ keV/m. The decrease above ∇T_{crit} must be very sharp, and is consistent with Eq. 3.5, and also with Eq. 3.2 if the value of γ exceeds 4; 'soft' transition functions do not fit these data. However, the flux-gradient relation is not unique; other gradient functions such as ∇p , $\nabla p/n$ or $1/n_e^2 \nabla n \nabla p$ also give double-valued functions. The 'threshold' gradients tend to show more variation in these cases, and the experimental curves more scatter. While we have not explicitly considered the influence of second order derivatives, it is worth noting that all of the flux-gradient relations considered are double-valued, while Ref. 13 implies that sufficiently

strong curvature terms could render the dependences monotonic. It may well be that second and first derivatives are strongly correlated, at least well away from the transition times. The technique used in this paper is a useful means of experimentally exploring the nonlinear structure of the fluxes and testing predictions of H-mode transition models. This approach hopefully will lead to more specific predictions, allowing us to distinguish clearly between various possible driving fluxes and gradients. It should be noted that the results presented here, in which power flux triggers the L-H transition, do not preclude other triggers in different experimental scenarios, such as the pellet-induced H-modes on DIII-D¹⁸.

Further work will include extending the range of global parameters in the power ramp experiments, and combining more discharges to reduce the scatter in measured gradients. We will also explore in more detail the fast evolution in the first few ms after the L-H transition, to try to understand better the time response under different plasma conditions.

References

- ¹Burrell K H 1997 *Phys. Plasmas* **4**, 1499.
- ²Yoshizawa A, Itoh S.-I, Itoh K and Yokoi N 2001 *Plasma Phys. Control. Fusion* **43**, R1.
- ³Hutchinson I.H., *et al.* 1994 *Phys. Plasmas* **1** 1511.
- ⁴Greenwald M, *et al* 1999 *Physics of Plasmas* **6**(5), 1943-9.
- ⁵Hubbard A E, Boivin R L, Granetz R S *et al* 2001 *Phys. Plasmas* **8** (5), 2033-2040.
- ⁶Hughes J W, Mossessian D A, Hubbard A E *et al* 2001 *Rev. Sci. Instrum.* **72**, 1107.
- ⁷Connor J W and Wilson H R 2000 *Plasma Phys. Control. Fusion* **42**, R1-R74
- ⁸Hubbard A E, *et al.*, 1998 *Plasma Physics Control. Fusion* **40** (5), 689-92.
- ⁹Groebner R J, Thomas D M and Deranian R D, 2001 *Phys. Plasmas* **8**(6), 2722.
- ¹⁰Hinton F L 1991 *Phys. Fluids B* **3**, 696.
- ¹¹Hinton F L and Staebler G M 1993 *Phys. Fluids B* **5**, 1281.
- ¹²Carreras B A, Newman D, Diamond P H and Liang Y-M 1994 *Phys. Plasmas* **1**, 4014.
- ¹³Taylor J B, Connor J W and Helander P 1998 *Phys. Plasmas* **5**, 3065.
- ¹⁴Diamond P H, Lebedev V B, Newman D E and Carreras B A 1995 *Phys. Plasmas* **2**, 3685.
- ¹⁵Lebedev V B and Diamond P H 1997 *Phys. Plasmas* **4**, 1087-1096.
- ¹⁶Barenblatt G I, "Scaling, self-similarity, and intermediate asymptotics", 1996 Cambridge University Press, Cambridge, England.
- ¹⁷Suttrop W, *et al.*, 1997, *Plasma Phys. Control. Fusion* **39** 2051-2066.
- ¹⁸Gohil P, *et al.*, 2001, *Phys. Rev. Lett.* **86**, 644.

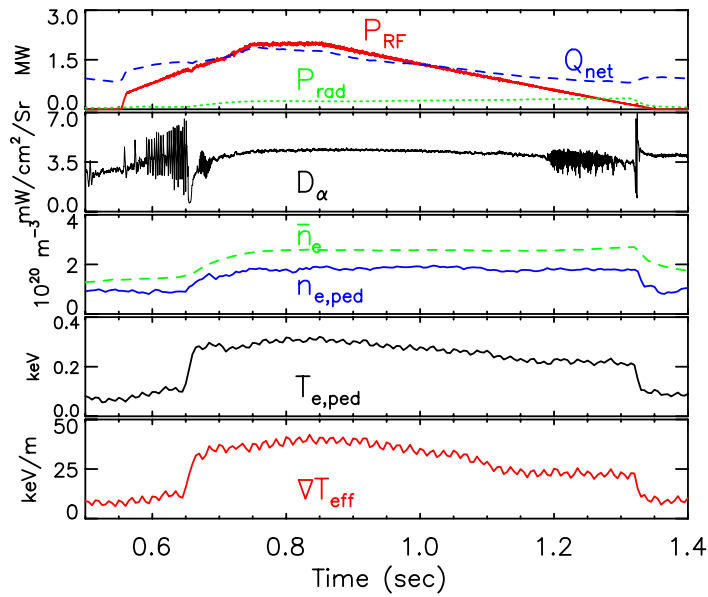


Figure 1: Time traces for a typical C-Mod power ramp discharge, 990915013. Top panel (a), shows launched RF power (solid), core radiation (dotted curve) and net power (dashed). (b) Horizontal D_α emission, showing transition to EDA H-mode at 0.654 secs, and back transition at 1.324 secs. (c) $n_{e,ped}$ from VB (solid) and line averaged density (dashed). (d) $T_{e,ped}$ from ECE. (e) average pedestal gradient $-\nabla T_{eff}$

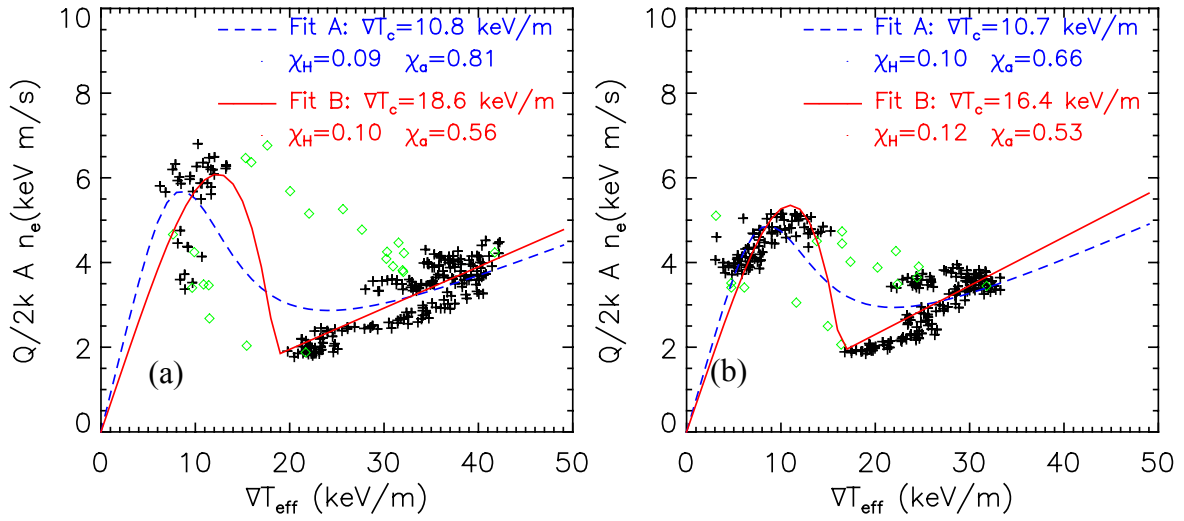


Figure 2 Normalized power flux $Q/2kAn_{e,ped}$ vs $-\nabla T_{eff}$ for two different densities (a) $\bar{n}_e = 1.1 \times 10^{20} m^{-3}$ (two discharges including that in Fig. 1), (b) $\bar{n}_e = 2.2 \times 10^{20} m^{-3}$. Only the slowly varying points (+) are used in fitting the model predictions of Eq. 3.2 (dashed) and Eq. 3.5 (solid).

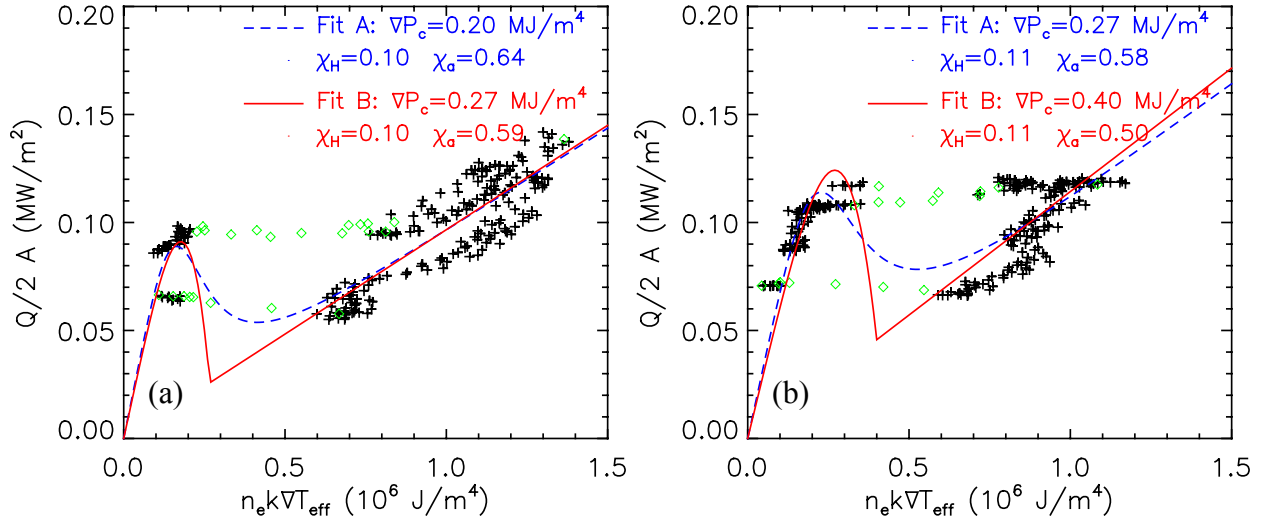


Figure 3. $Q/2A$ vs $-n_{e,ped}k\nabla T_{eff}$, for the same dataset as in Fig. 2. The curves represent the same equations, but with the new dependent variable.

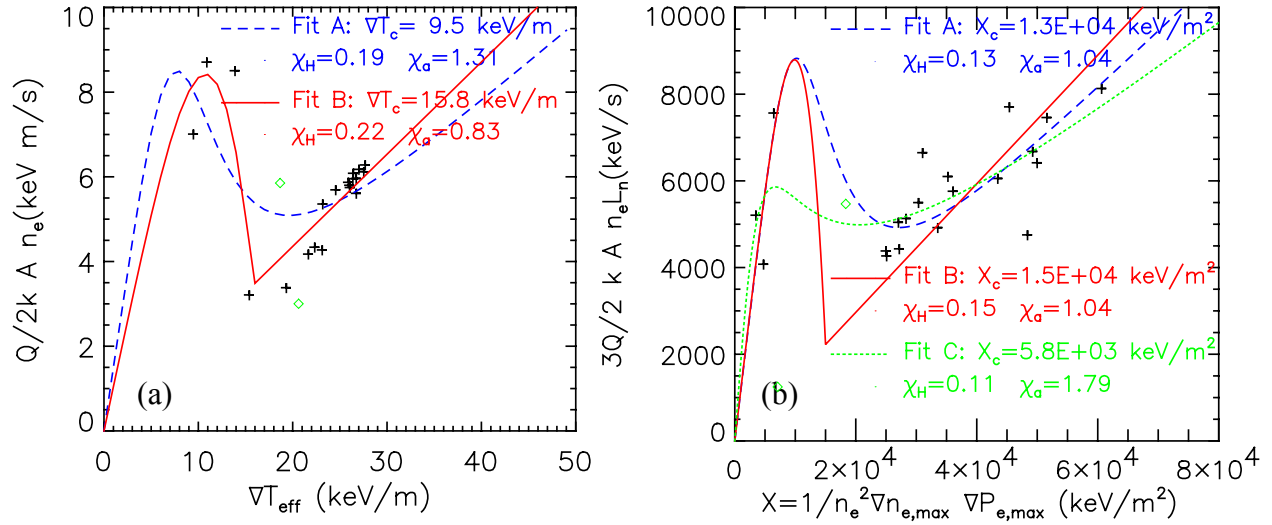


Figure 4: Data from ETS for power ramp discharge 1010726018 with $\bar{n}_e = 1.6 \times 10^{20} \text{ m}^{-3}$.
 (a) $Q/2kAn_{e,\text{mid}}$ vs $-\nabla T_{\text{max}}$, showing similar relations and critical gradient to those in Fig. 2.
 (b) Renormalized flux $3Q/2kAn_e L_n$ vs $1/n_e^2 (dn_e/dr)_{\text{max}} (dp_e/dr)_{\text{max}}$, for comparison with Ref. 11. The dotted curve is for $\gamma=2$, while the solid and dashed curves are for the same functions as in previous fits.